

Discover Physical Concepts and Equations with Machine Learning

Bao-Bing Li¹, Yi Gu^{2,*}, and Shao-Feng Wu^{1,3}

¹*Department of Physics, Shanghai University, 200444 Shanghai, China*

²*Department of Physics, Ludwig-Maximilians-Universität, 80333 Munich, Germany*

³*Center for Gravitation and Cosmology, Yangzhou University, 225009 Yangzhou, China*

**E-mail: Gu.Yi@campus.lmu.de*

Abstract

Machine learning can uncover physical concepts or physical equations when prior knowledge from another one is available. However, in many cases, these two aspects are coupled and cannot be discovered independently. We extend *SciNet*, which is a neural network architecture that simulates the human physical reasoning process for physics discovery, by proposing a model that combines Variational Autoencoders (VAEs) with Neural Ordinary Differential Equations (Neural ODEs). This allows us to simultaneously discover physical concepts and governing equations from simulated experimental data across diverse physical systems. We apply the model to several key examples inspired by the history of physics, including Copernicus' heliocentric solar system, Newton's law of universal gravitation, the wave function together with the Schrödinger equation, and spin-1/2 along with the Pauli equation. The results demonstrate that the neural network successfully reconstructs the corresponding theories.

1 Introduction

Einstein famously argued that “It can scarcely be denied that the supreme goal of all theory is to make the irreducible basic elements as simple and as few as possible without having to surrender the adequate representation of a single datum of experience” [1]. The basic elements of physical theories are physical concepts and equations. Finding simple and elegant physical concepts and equations that can fully describe experimental phenomena has always been the goal of theoretical physicists.

Physics typically advances by building upon existing theories, incorporating new experimental phenomena and mathematical tools to expand them. However, when confronting revolutionary problems, inherited theories may not naturally describe new phenomena. In such cases, breakthrough discoveries are needed to revise the old theories, and this can be a long process. For example, it took several centuries to transition from the geocentric model to the heliocentric model, and nearly 30 years from Planck’s quantum hypothesis to the Schrödinger equation. Moreover, human research into new phenomena relies on the current level of experimental capability and physical understanding. Subtle physical mechanisms, such as spin, may already be hidden within the data, but they are not easily discovered [2].

In recent years, the emerging field of AI for Science has developed rapidly, helping researchers gain insights unattainable by traditional scientific methods [3–5]. As a research assistant tool, AI has made significant contributions in various areas of physics, such as cosmology [6–14], high-energy physics [15–21], string theory [22–26], and condensed matter physics [27–31]. Beyond achieving success in these specific areas of physics, recent works [32–38] have demonstrated that AI is capable of conducting independent and autonomous research in general physics. Important physical concepts [39, 40], physical properties such as symmetries [41, 42], and physical laws such as Kepler’s laws [43], Newton’s laws [44] and conservation laws [45–47] can all be discovered by AI from data. Analytic physical equations can not only be directly obtained through symbolic regression [48–50], but can also be derived by causal inference based on a set of prior knowledge [43, 51]. In the study of dynamical systems, purely machine learning methods [52–55] have been widely used to analyze complex systems [56–59] and solve engineering problems [60–62]. In parallel, physics-inspired approaches [63–67] have also made substantial progress. Although not formally defined, AI is expected to become the fifth paradigm of scientific research [68].

Science is the attempt at the posterior reconstruction of existence by the process of conceptualization [69]. *SciNet*, proposed by Iten et al. [40], is an important neural network model that autonomously discovers physical concepts from data without requiring

prior knowledge. The techniques for discovering equations have also been widely applied in various fields of physics [35, 70–72]. However, in physics, many concepts and equations are coupled and hard to discover independently. Without physical concepts, it is evidently impossible to determine the governing physical equations. Conversely, without physical equations, our understanding of physical concepts remains localized, leaving us unable to discern their temporal and spatial evolution. For example, Schrödinger introduced the concept of the wave function and proposed the Schrödinger equation simultaneously when explaining the behavior of quantum particles [73]. Current machine learning models mainly focus on discovering either physical concepts or physical equations and often require prior knowledge about the other. We adopted the questioning mechanism from *SciNet* and replaced the uniform evolution of latent representations, which was limited to specific systems, with Neural Ordinary Differential Equations [74]. We do not rely on any prior knowledge specific to particular examples, instead making the natural assumption that the evolution of physical concepts is governed by differential equations. This enhancement renders the framework more general, enabling the simultaneous discovery of physical concepts and governing equations. Although previous works [75–78] have applied similar models in some specific tasks, they mainly focused on the predictive power of neural networks, whereas our goal is to extract meaningful physical information from the latent representations. We are particularly concerned with whether important concepts and equations in the history of theoretical physics can be discovered. We apply our model to four examples in physics: Copernicus’ heliocentric solar system, Newton’s law of universal gravitation, wave function with the Schrödinger equation, and spin-1/2 with the Pauli equation. Despite the redundancy in the latent space, we find that AI can still identify those physical theories in textbooks.

The first three examples refer to previous works [39, 40, 79]. Compared to their models, which aim to identify either concepts or equations or are designed for specific systems, our model can simultaneously discover both across different systems. In the case of the Copernicus’ heliocentric solar system, *SciNet* utilized an implicit questioning mechanism (e.g., “where is the particle at time t' ?”) [40] by providing sequentially ordered observational data. We use the same mechanism in the first example. However, in the following three examples, an explicit questioning mechanism regarding control variables such as potential fields is used (e.g., “where is the particle at time t' under potential field V' ?”). This allows the model to handle systems with additional control variables, thereby extending its applicability. Specifically, in the example of spin-1/2 with the Pauli equation, even when

physical concepts have higher dimensions than the observational data, AI can still effectively reconstruct the actual theory. Compared to the step-by-step exploration of physics by humans, end-to-end AI has the ability to directly discover hidden features and intrinsic patterns from data, thus relying less on prior knowledge. This helps to discover physical mechanisms that might have been overlooked.

The rest of the paper will be arranged as follows. Section 2 introduces our neural network architecture that mimics human physical modeling. In Section 3, we describe the four physical examples and analyze the training results. Conclusions are presented in Section 4. Additionally, there are five appendices. In Appendix A, we provide a detailed analytical derivation of the loss function. Appendix B introduces knowledge about random potential functions. In Appendix C, we compare the results of the Stern-Gerlach experiment under non-uniform and uniform magnetic fields. Appendix D provides detailed information on the neural network architecture and the training process. In Appendix E, we analyze the multivariable linear system.

2 Method

The development of physical theories begins with the observation of natural phenomena. Physical data serve as the foundation for constructing theories. Such data often originate from direct experimental observations or from indirect methods of data generation, offering the essential facts and phenomena upon which theories are built. Physicists analyze these data to propose physical concepts, such as particles, waves, and fields, and formulate equations to explain the observed phenomena. The development of these concepts and equations is an intertwined process, with their mathematical form providing a quantitative and predictive framework for accurately describing physical laws. Throughout this process, physicists refine theoretical models by posing questions, such as, “What would happen if we altered a specific condition?” and seeking answers. When experimental results support the theory, it is reinforced; when they contradict the predictions, the theory may need to be revised.

To develop a general machine learning-based method for physics research, we model our approach on the way human physicists construct physical theories, as illustrated in Figure 1. We consider sequential observational data $(t_i, O(t_i))$, which describe the evolution of the system over time or space. Direct observational data are often difficult for humans to interpret. We assume that there exists a physical theory capable of describing the

observed data in a simple yet comprehensive manner. Physical concepts in this theory are represented by $C(t_i)$, whose behavior is governed by the differential equation $dC/dt = f(C, t, V)$, where V represents experimental conditions or environmental variables. Altering V is akin to posing a series of “questions” about the physical system. By adjusting V and observing how $C(t_i)$ evolves, we can assess the accuracy and applicability of the theory. Our target is to apply machine learning techniques to identify such physical concepts and their corresponding differential equations.

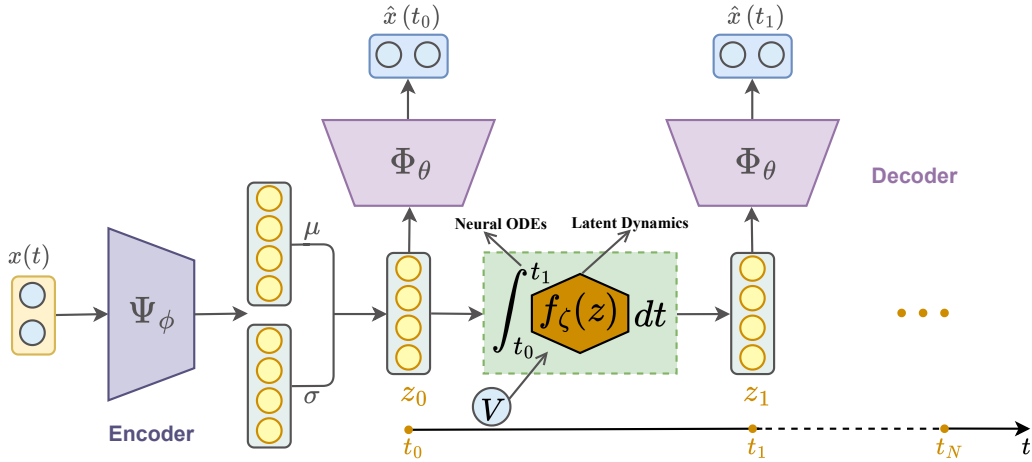


Figure 1: Neural Network Architecture. Our model consists of two parts: Variational Autoencoders and Neural ODEs. The observed data $\mathbf{x}(t)$ is processed by the encoder Ψ_ϕ , which outputs the distribution parameters $\boldsymbol{\mu}$ and $\boldsymbol{\sigma}$ in the latent space. Then, an initial latent state $\mathbf{z}(t_0)$ is sampled from $\boldsymbol{\mu}$, which is used as input to Neural ODEs. The equations represented by Neural ODEs are related to initial latent state $\mathbf{z}(t_0)$ and an adjustable control variable V . Using an ODE solver, it outputs a series of latent states at different time points $\mathbf{z}(t_i)$. These latent states are then reconstructed by the decoder Φ_θ to produce the corresponding observed data $\hat{\mathbf{x}}(t_i)$ at each time point.

Discovering Physical Concepts.—Suppose there is a connection between the direct observational data and the underlying physical concepts, such that there exists a mapping $E : \mathcal{O} \rightarrow \mathcal{C}$ and an inverse mapping $D : \mathcal{C} \rightarrow \mathcal{O}$. We use a Variational Autoencoders [80] to learn the mappings E and D between the observational data and the physical concepts. VAEs consist of a probabilistic encoder and a probabilistic decoder. The probabilistic encoder maps input data space to a continuous latent space, producing latent representations. The probabilistic decoder then uses these latent representations to reconstruct the input data or generate new data. The latent representations \mathbf{z} are sampled from a multi-dimensional Gaussian distribution, given the data \mathbf{x} and the probabilistic encoder. These representations capture the essential features and internal structure of the data. In physics,

physical concepts serve as a simple and essential representation of the physical observational data. When we input observational data into VAEs, we expect the latent space to store information corresponding to these core physical concepts. However, the latent space of VAEs can exhibit redundancy [81–83], meaning it may capture secondary information. Previous studies [40, 84–87] have shown that incorporating KL divergence as a regularization term can effectively address this issue by encouraging the latent space to capture minimal, sufficient, and uncorrelated representations. The expression for KL divergence is as follows:

$$L_{KL}(\mathbf{x}; \phi, \zeta, \theta) = D_{KL}(q_{\phi}(\mathbf{z}|\mathbf{x})||p_{\theta}(\mathbf{z})). \quad (1)$$

Based on this insight, we incorporate KL divergence into our architecture to optimize the latent space representation, bringing it closer to the requirements of physics.

Discovering Physical Equations.—The dynamical equations that govern the evolution of physical concepts are another essential element of theory. Several machine learning techniques have been developed to identify the underlying governing equations from sequential data, including Recurrent Neural Networks (RNNs) [88], Graph Neural Networks (GNNs) [89], SINDy [34], and Koopman Theory [90]. In this work, we utilize Neural Ordinary Differential Equations (Neural ODEs) to discover physical equations. Neural ODEs are a class of machine learning models that integrate traditional neural networks with Ordinary Differential Equations (ODEs). Unlike discrete-time models such as RNNs, Neural ODEs can model dynamical systems in a continuous time domain. Since neural networks are capable of approximating any function, Neural ODEs are particularly well-suited for handling nonlinear dynamics, outperforming methods like Koopman Theory and SINDy, which require specific candidate functions and additional hyperparameters.

The governing equations of many dynamical systems can be represented by ordinary differential equations, in the general form:

$$\frac{dy(t)}{dt} = f(t, y(t)) \approx NN(t, y(t)), \quad (2)$$

where t is time, $y(t)$ are state variables, and f is the function determined by the ODEs. Neural ODEs use a neural network NN to approximate the function f . Once f is found, the governing equation of the system is determined.

Given an initial value for the state variable $y(t_0)$ and a randomly initialized neural network NN , Neural ODEs use a black-box ODE solver to find the state variable at any time step through forward propagation:

$$\hat{y}(t_1) = y(t_0) + \int_{t_0}^{t_1} NN(t, \hat{y}(t)) dt, \quad (3)$$

We take the actual trajectory of the state variable $y(t)$ within a specified time range as the target data and compute its difference with the generated trajectory $\hat{y}(t)$. Then, we use backpropagation to optimize the neural network parameters to approximate the true function f .

The backpropagation of Neural ODEs is implemented using the adjoint sensitivity method [74]. Suppose there is a loss function dependent on the output of the ODE solver:

$$L(y(t_1)) = L(y(t_0)) + \int_{t_0}^{t_1} NN(t, y(t); \zeta) dt. \quad (4)$$

The adjoint state is defined as:

$$a(t) = \frac{\partial L}{\partial y(t)}, \quad (5)$$

It has been proven that the adjoint dynamics are governed by another ordinary differential equation [74]:

$$\frac{da(t)}{dt} = -a(t) \cdot \frac{\partial NN}{\partial y}, \quad (6)$$

The parameter gradient can be calculated using integration:

$$\frac{\partial L}{\partial \zeta} = \int_{t_1}^{t_0} a(t) \cdot \frac{\partial NN}{\partial \zeta} dt. \quad (7)$$

Neural ODEs work in a continuous-time framework, which makes them well-suited for modeling physical processes that evolve continuously over time. They can learn the smooth transition from one state to another while being more efficient in terms of the number of parameters. Neural ODEs have found many applications in different fields of physics [91–95].

Forward Propagation.—In our architecture, the forward propagation of data is illustrated in Figure 1. We begin by considering the sequential observation data in the observable space \mathcal{X} , denoted as $\{\mathbf{x}(t_i)\} = \{\mathbf{x}(t_0), \mathbf{x}(t_1), \dots, \mathbf{x}(t_T)\}$, which describes the evolution of the observational data over time. This data is input into the probabilistic encoder Ψ_ϕ . The encoder Ψ_ϕ outputs a probability distribution in the latent space, represented by the mean $\boldsymbol{\mu}$ and variance $\boldsymbol{\sigma}$:

$$(\boldsymbol{\mu}_\phi, \boldsymbol{\sigma}_\phi^2) = \Psi_\phi(x). \quad (8)$$

Next, we sample from the mean $\boldsymbol{\mu}$ to obtain the latent representation at the first time step $\mathbf{z}(t_0)$:

$$\mathbf{z}(t_0) = \boldsymbol{\mu}, \quad (9)$$

Sampling only from the mean $\boldsymbol{\mu}$ is a common practice [96–98]. Here, \mathbf{z} is vector whose dimension is the same with that of the latent space.

We use Neural ODEs to define the dynamics of the latent representation through a differential equation to be learned:

$$\frac{dz(t)}{dt} = NN(t, z(t), V; \zeta). \quad (10)$$

Here, the neural network NN that governs the differential equation takes time t , the state variable $z(t)$, and an optional control variable V representing other essential conditions as inputs. For example, V could represent the potential field controlling the motion of particles. This can also be interpreted as a questioning mechanism, where the neural network is tasked with predicting the observed data at a specific time t based on the potential function V .

We treat $z(t_0)$ as the initial condition for Neural ODEs and employ a black-box solver to compute the latent representations at the subsequent T time steps:

$$\{z(t_i)\} = \{z(t_0), z(t_1), \dots, z(t_T)\}. \quad (11)$$

The decoder Φ_θ then takes the trajectory of the latent representation and reconstructs the corresponding observed data at each time step:

$$\hat{\mathbf{x}}(t_i) = \{\hat{\mathbf{x}}(t_0), \hat{\mathbf{x}}(t_1), \dots, \hat{\mathbf{x}}(t_T)\}. \quad (12)$$

The encoder Ψ_ϕ , decoder Φ_θ , and the neural network function NN of Neural ODEs in our model are all fully connected networks consisting of multiple hidden layers and nonlinear activation functions. Additional details can be found in Appendix D.

Loss Function.—We quantify the discrepancy between the physical theories discovered by the machine and the actual physical theories by calculating the error between the reconstructed data $\hat{\mathbf{x}}(t)$ and the true observational data $\mathbf{x}(t)$. This process is analogous to how physicists refine theories based on comparative experimental results. Using the gradient descent algorithm [99], the neural network model iteratively updates the parameters representing the learned theory, minimizing the reconstruction error to ultimately identify a physical theory that adequately describes the observed phenomena. The Mean Squared Error (MSE) is used as the metric for measuring reconstruction error. In combination with the KL divergence in VAEs, our overall loss function is expressed as:

$$L(\mathbf{x}; \phi, \zeta, \theta) = \frac{1}{N} \sum_{i=1}^N [(\mathbf{x}(t_i) - \hat{\mathbf{x}}(t_i))^2] + \beta \cdot D_{KL}(q_\phi(\mathbf{z}|\mathbf{x})||p_\theta(\mathbf{z})). \quad (13)$$

where β is a hyperparameter that controls the influence of the regularization term on the overall optimization objective. This parameter helps balance the model’s reconstruction accuracy with the independence of the learned latent representations. Further details on

the derivation of the loss function, neural network initialization, optimization methods, and parameters used during the training process are provided in Appendix A.

Train Strategies.—There are another two key hyperparameters in our model: the dimension of the latent space and the order of the differential equations in Neural ODEs. These hyperparameters correspond to the number of physical concepts required to describe the phenomena and the basic form of the governing physical equations, respectively. To maintain objectivity in the neural network model, we do not assume prior knowledge of these parameters but treat them as hyperparameters to be determined during the formal training process. We identify the optimal values by comparing experimental results under different settings.

1. **Number of Physical Concepts:** We train models with different latent space dimensions under the same conditions and plot the corresponding loss function curves. According to Occam’s Razor, the optimal physical concepts should fully describe the observed data using the smallest possible number. Therefore, we select the smallest latent space dimension that does not result in a significant increase in the loss function as the number of physical concepts.
2. **Determining the Form of the Differential Equation:** While Neural ODEs can capture the dynamical equations underlying complex data, they typically cannot automatically infer the fundamental mathematical structure of the differential equations, such as their order. Therefore, we treat the order of the differential equation as a hyperparameter. By explicitly specifying the order, we can guide Neural ODEs to more accurately learn the specific form of the differential equation. During training, we start with the most general assumption that the differential equations are first-order and use the aforementioned ablation experiments to determine the number of physical concepts. For simple systems, first-order differential equations are often sufficient. However, for more complex systems, when the model’s performance is suboptimal, we can iteratively impose additional universal constraints, such as symmetry or the grouping of differential equations, to fine-tune the model and ultimately identify the optimal physical theory.

3 Results

We choose four representative physical examples: Copernicus’ heliocentric solar system, Newton’s law of universal gravitation, and one-dimensional quantum systems governed by

the Schrödinger equation and the Pauli equation. By comparing the experimental results with physical theories, we have found that the neural network can identify important physical concepts and equations.

3.1 Copernicus’ heliocentric solar system

Copernicus’ heliocentric solar system holds a very important place in history, marking a major shift in humanity’s understanding of the universe. These scientific achievements are not only milestones in astronomy but also signify a general research paradigm in physics that starts from observational data and seeks to discover universal and effective physical laws through simplicity and predictability. Here, we consider the Copernicus’ heliocentric solar system where Mars and Earth orbit the Sun in uniform circular motion, as shown in Figure 2(a). The key question then becomes: Can AI, without any prior knowledge, replicate the work of Copernicus? This would be an essential first step for AI to discover even more complex physical theories.

As shown in Figure 2(a), the distance between Earth and Mars is given by:

$$d = \sqrt{R_E^2 + R_M^2 - 2 \cdot R_E \cdot R_M \cdot \cos(\phi_E + \phi_M)}. \quad (14)$$

where R_E is the average distance from the Earth to the Sun, and R_M is the average distance from Mars to the Sun. With distant celestial bodies as the reference frame, ϕ_E and ϕ_M are the angles of Earth and Mars relative to the Sun, respectively. Then, the angles of the Sun and Mars relative to the Earth, θ_S and θ_M , are given by:

$$\theta_S = \pi - \phi_E, \quad (15)$$

$$\theta_M = \text{angle}(\text{complex}(\cos(\theta_M), \sin(\theta_M)))^1, \quad (16)$$

where

$$\cos(\theta_M) = \frac{R_M \cos(\phi_M) - R_E \cos(\phi_E)}{d}, \quad (17)$$

$$\sin(\theta_M) = \frac{R_E \sin(\phi_E) + R_M \sin(\phi_M)}{d}, \quad (18)$$

In work [40], Iten et al. introduced a powerful neural network model called *SciNet* which is designed to mimic the human reasoning process. They successfully enabled the neural network to autonomously discover the concept of heliocentric angles from time-evolving

¹Expression(16) is defined in the code and is used to compute the phase angle of a complex number from its real and imaginary components. In programming, complex numbers are represented by their real and imaginary parts, and the function “*angle*” calculates the polar angle, providing the value of θ_M .

geocentric angle data by assuming that the physical concepts hidden in the data evolve uniformly over time. Although uniform motion is a very natural assumption, we hope to relax these prior assumptions and only presume that the latent variables evolve through differential equations, which is more general, expecting the neural network to discover physical concepts and corresponding physical equations in a more autonomous manner from the data.

Our physical setup is the same as in [40]. The training dataset consists of randomly selected subsequences of geocentric angles $\theta_M(t)$ and $\theta_S(t)$ recorded weekly throughout Copernicus’s entire lifespan, totaling 3665 observations. The neural network’s input data are the geocentric angles at the first time step $\theta_S(t_0)$ and $\theta_M(t_0)$, with label data being the geocentric angles for the subsequent 50 time steps. The differential equations to be discovered are set as:

$$\frac{d\mathbf{h}(t)}{dt} = NN(\mathbf{h}(t); \zeta). \quad (19)$$

$NN(\mathbf{h}(t); \zeta)$ is a neural network parameterized by ζ and inputted by $\mathbf{h}(t)$.

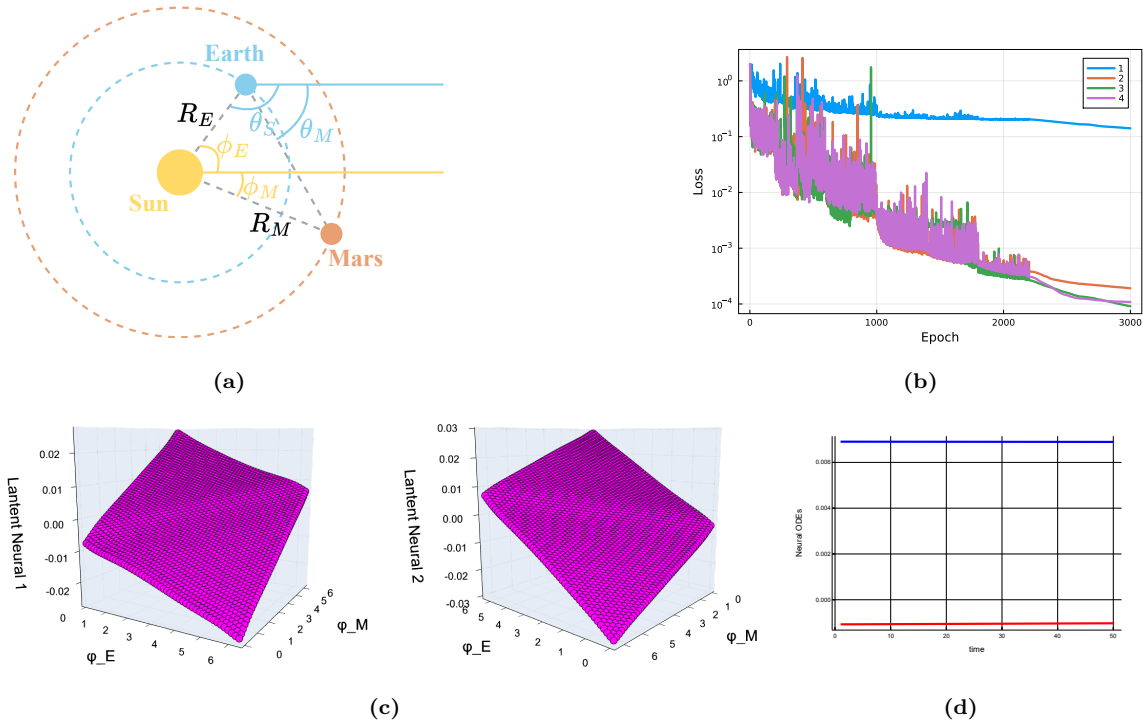


Figure 2: Heliocentric solar system. (a) Positions and motions of Earth and Mars relative to the Sun. (b) Impact of latent dimensions on loss, showing a two-dimensional space as optimal. (c) Latent representations capture linear combinations of heliocentric angles of Earth and Mars. (d) The differential equation learned indicates constant rates of change for the heliocentric angles.

Ablation experiments show, as depicted in Figure 2(b), that although the loss is slightly

lower in three-dimensional and four-dimensional latent spaces compared to the two-dimensional space, the two-dimensional space maintains the minimum representation necessary to describe the physical system with its much lower loss than one-dimensional space. Therefore, we consider the optimal latent dimension for the system to be two. Figure 2(c) displays the representations learned by the neural network: the two latent representations store a linear combination of the true heliocentric angles ϕ_E and ϕ_M . This indicates that the neural network successfully discovers the concepts of two heliocentric angles from the observed angles of the Sun and Mars from Earth. Figure 2(d) shows that the learned neural networks $NN(\mathbf{h}(t); \zeta)$ in Neural ODEs are two constants, indicating that the two heliocentric angles are evolving at a constant speed, which is consistent with the actual setting. These results prove that our model successfully rediscovers the concept of heliocentric angles and their laws of motion from geocentric angle data.

3.2 Newton’s Law of Universal Gravitation

Newton’s law of universal gravitation provides methods for the accurate prediction of celestial orbits based on a minimal amount of observational data, allowing for the calculation of long-period celestial motions. Against this background, we hope that artificial intelligence can automatically identify the law of universal gravitation from limited observational data without prior knowledge of the specific physical principles.

In [79], an adaptive method called *Sir Isaac* was developed, which derived Newton’s law of universal gravitation from simulated celestial motion data. We employ the same physical setup as in [79], simulating an object with mass m moving under a gravitational field by another central body with mass M where $M \gg m$. The evolution of the distance $r(t)$ between them follows the dynamic equation:

$$\frac{d^2r}{dt^2} = \frac{h^2}{r^3} - \frac{GM}{r^2}, \quad (20)$$

where $h = (v_0 \cdot \hat{\theta})r_0$ is a specific angular momentum, v_0 is the initial velocity of moving object, r_0 is the initial distance, and $\hat{\theta}$ is a unit vector perpendicular to the line connecting the two masses, with G being the gravitational constant. Setting the initial velocity parallel to $\hat{\theta}$, GM/v_0^2 as the unit of distance and GM/v_0^3 as the unit of time, the dynamic equation simplifies to:

$$\frac{d^2r}{dt^2} = \frac{1}{r^2} \left(\frac{r_0^2}{r} - 1 \right). \quad (21)$$

The trajectory of its motion is shown in Figure 3(a). During the generation of training data, r_0 is uniformly sampled 1000 times between 1 and 3, covering all possible trajectory

types: circular when $r_0 = 1$; elliptical when $1 < r_0 < 2$; parabolic when $r_0 = 2$; and hyperbolic when $r_0 > 2$.

Initial distances r_0 serve as input data and control variables in the model to explore how the trajectories of objects change with different initial distances r_0 . The label data are distances $r(t)$ observed over the subsequent 100 time steps², as shown in Figure 3(b). The differential equations to be discovered are set as follows:

$$\frac{d\mathbf{h}(t)}{dt} = NN(\mathbf{h}(t), r_0; \zeta). \quad (22)$$

\mathbf{h} is a vector whose components are latent representations. The number of components is the same as the dimension of the latent space.

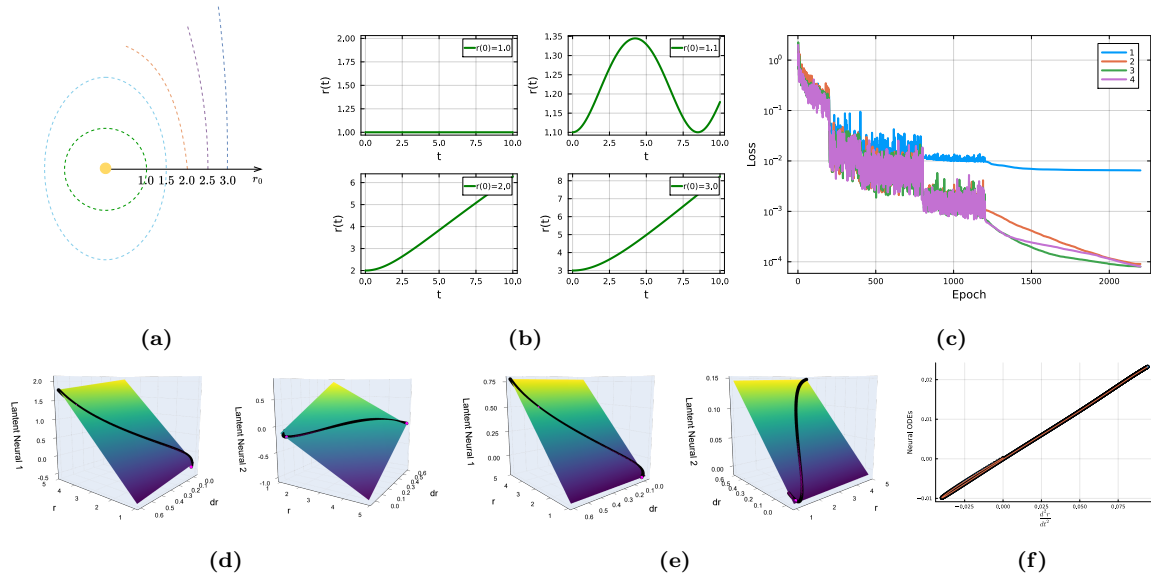


Figure 3: Law of Universal Gravitation. (a) Different types of trajectories determined by r_0 : When $r_0 = 1$, the orbit is circular; when $1 < r_0 < 2$, the orbit is elliptical; when $r_0 = 2$, the orbit is parabolic; when $r_0 > 2$, the orbit is hyperbolic. (b) Distribution of distances $r(t)$ from the central body corresponding to different r_0 . (c) Impact of latent dimensions on loss, showing that a two-dimensional space is optimal. (d) Latent representations with first-order differential equations store linear combinations of r and \dot{r} . (e) Latent representations with second-order differential equations capture r and \dot{r} independently. (f) Neural ODEs learn the differential equation of this system.

Ablation experiments show, as displayed in Figure 3(c), that the optimal number of physical concepts required to describe this physical system is two. Figure 3(d) shows the representation learned by the neural network: two latent representations store the linear

²In this example, we also incorporate the Mean Relative Error (MRE) as a regularization term into the loss function during training. This helps improve the accuracy of the learned concepts and equations, ensuring that the model minimizes relative deviations in its predictions.

combinations of the true distance r and the velocity \dot{r} , indicating that the neural network has discovered them as the optimal concepts for describing this physical system. Further, we aim to unravel this linear combination to obtain independent physical concepts. A reasonable guess is that the governing equations are second-order differential equations. To validate this hypothesis, we only need to set the two differential equations as:

$$\frac{dh_1(t)}{dt} = h_2(t), \quad (23)$$

$$\frac{dh_2(t)}{dt} = NN(h_1(t), h_2(t), r_0; \zeta). \quad (24)$$

h_1 and h_2 are the two components of \mathbf{h} .

At this point, Figure 3(e) shows that the two latent representations no longer store a linear combination of physical concepts, but instead independently discover the two physical concepts r and \dot{r} as follows:

$$h_1 = a_1 r + b_1, \quad (25)$$

$$h_2 = a_2 \frac{dr}{dt} + b_2, \quad (26)$$

As a result, the equation learned by Neural ODEs should be:

$$NN = \frac{dh_2}{dt} = \frac{d}{dt}(a_2 \cdot \frac{dr}{dt} + b_2) = a_2 \cdot \frac{d^2r}{dt^2} = a_2 \cdot \left[\frac{1}{r^2} \cdot \left(\frac{r_0^2}{r} - 1 \right) \right]. \quad (27)$$

where d^2r/dt^2 is the actual dynamical Eq.(21). As shown in the Figure 3(f), there is actually a linear relationship between the output NN learned by Neural ODEs (y-axis) and the theoretical dynamical equation d^2r/dt^2 (x-axis).³

3.3 Wave Function with the Schrödinger Equation

Wave function and the Schrödinger equation form the foundation of quantum mechanics. Here, we are curious whether machine can discover them without knowing quantum mechanics itself. Wang et al. [39] proposed an introspective recurrent neural network architecture, called “the Schrödinger machine”, which includes a translator and a knowledge distiller. By using a two-stage method that involves Taylor expansion and linear projection to update its hidden states and generate outputs, it could extract the concept of quantum wave functions and the Schrödinger equation⁴. Their model is specifically designed for this

³Due to the non-monotonic variation of the motion equation d^2r/dt^2 with respect to r , ideally, it should appear as a perfectly coincident straight line in the graph. However, the inherent small errors of the neural network when learning such complex dynamics result in the theoretically coincident lines appearing as two nearly parallel lines in the graph.

⁴This process can be explained by Koopman theory.

particular example. We want to use our more generalizable model to accomplish this task while enhancing its interpretability.

In this regard, we adopt the same physical setting as in [39], considering a single quantum particle moving in one-dimensional space with a specific potential function. Scientists can collect density distributions of Bose-Einstein condensates (BEC) in potential traps of various shapes through cold atom experiments.

The Schrödinger equation describes the quantum state of microscopic particles. In one dimension, its stationary form is given by:

$$-\frac{\hbar^2}{2m} \frac{d^2\psi(x)}{dx^2} + V(x)\psi(x) = E\psi(x). \quad (28)$$

We introduce 2000 sets of random potential functions $V_i(x)$ ($i = 1, 2, \dots, 2000$), keeping $V_i < 0$ to ensure that the particles remain in a bound state. For details on the random potential functions, see Appendix B. We assume that the potential energy is always measured relative to the particle’s energy, which is effectively set to zero. The simplified equation can be written as:

$$\frac{d^2}{dx^2}\psi_i(x) = V_i(x)\psi_i(x), \quad (29)$$

The density distribution $\rho_i(x)$ is defined as:

$$\rho_i(x) = |\psi_i(x)|^2. \quad (30)$$

We initialize both the wave function and its derivative with a value of 1, evolve them over position x , and calculate the corresponding probability density at each position step to generate the training data. The input and label data are the trajectories of all 2000 sets of density distribution $\rho_i(x)$ observed in the next 50 position steps. Figure 4(a) displays two sets of random potential functions $V_i(x)$ and their corresponding trajectories of density distributions $\rho_i(x)$. The differential equations to be discovered are set as:

$$\frac{d\mathbf{h}(x)}{dx} = NN(\mathbf{h}(x), V; \zeta). \quad (31)$$

Here, V is a control variable.

Ablation experiments, as shown in Figure 4(b), indicate that the optimal number of physical concepts is two, a conclusion consistent with the results reported in [39]. Figure 4(c) shows that under the assumption of first-order differential equations, the learned representations store linear combinations of the actual wave function ψ and its derivative $\dot{\psi}$. This suggests that the neural network has identified the wave function and its derivative as the optimal concepts for describing this physical system. Furthermore, we attempt to use

second-order differential equations as an assumption to unravel these linear combinations. Similar to the previous example, the differential equations are:

$$\frac{dh_1(x)}{dx} = h_2(x), \quad (32)$$

$$\frac{dh_2(x)}{dx} = NN(h_1(x), h_2(x), V; \zeta). \quad (33)$$

h_1 and h_2 are the two components of \mathbf{h} .

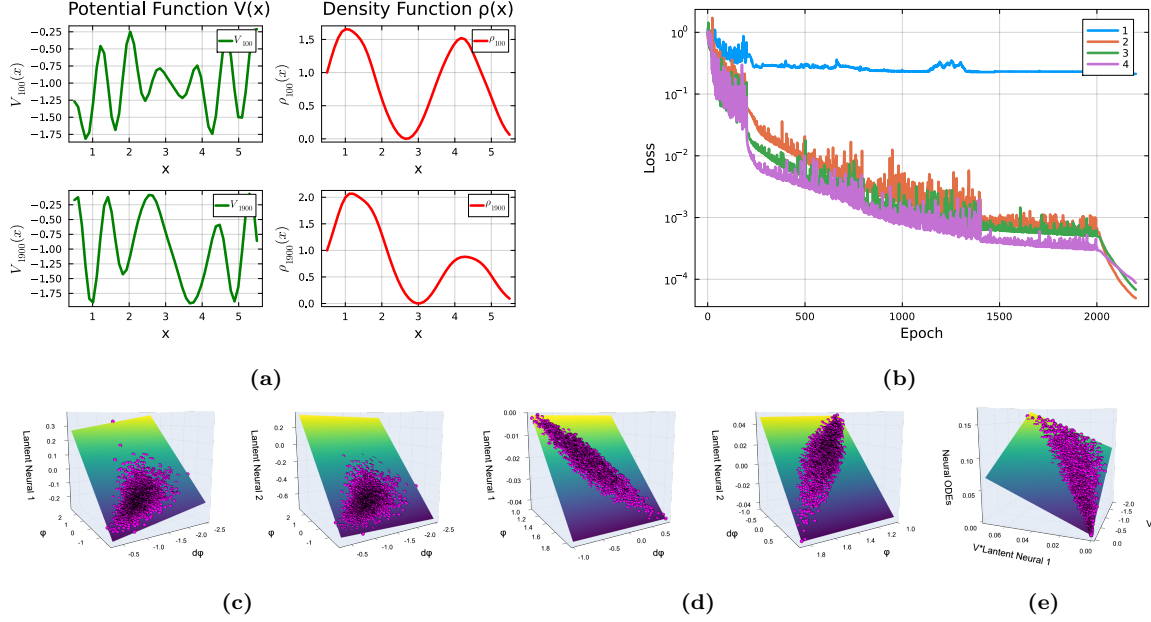


Figure 4: The Schrödinger Equation Model. (a) Random potentials (green) and corresponding density distributions (red). (b) Impact of latent dimensions on loss, showing a two-dimensional space as optimal. (c) Latent representations with a first-order differential equation store linear combinations of the wave function and its derivative. (d) Latent representations with a second-order differential equation capture wave function and its derivative independently. (e) Successful learning of the system’s second-order differential equation by Neural ODEs.

Figure 4(d) shows what the two latent representations h_1 and h_2 now correspond to the wave function and its derivative, uncoupled from each other. They differ from the true physical quantities only by a linear transformation:

$$h_1 = a_1 \cdot \psi + b_1, \quad (34)$$

$$h_2 = a_2 \cdot \frac{d\psi}{dx} + b_2. \quad (35)$$

By calculating the derivatives with respect to space, we can obtain:

$$NN = \frac{dh_2}{dx} = \frac{a_2}{a_1} \cdot (V \cdot h_1) - \frac{a_2 \cdot b_1}{a_1} \cdot (V). \quad (36)$$

As shown in Figure 4(e), the learned output NN of Neural ODEs (z -axis) is plotted against $V \cdot h_1$ (x -axis) and V (y -axis). The plot clearly reveals a linear relationship among these variables, indicating that Neural ODEs have effectively captured the underlying spatial dynamical equation.

3.4 Spin-1/2 with the Pauli Equation

The Stern-Gerlach experiment in 1922 revealed the splitting of silver atom trajectories in a non-uniform magnetic field, challenging classical physics and prompting Pauli in 1924 to propose the concept of two-valuedness. This idea became the foundation of the Pauli exclusion principle. In 1925, Uhlenbeck and Goudsmit introduced the notion of electron spin, which Pauli later integrated into quantum mechanics, leading to the development of spin theory, the introduction of Pauli matrices, and the two-component spin wave function.

Now, let us consider the following scenario: if the Stern-Gerlach experiment had employed a uniform magnetic field, only a single stripe would have appeared on the screen, as illustrated in Figure 5(a). Such a setup would likely have masked the quantization of angular momentum. However, spin and the Pauli equation describe intrinsic properties and fundamental laws of particles, which remain present and operative, even if they are not directly observable in experimental data. Without the angular momentum quantization revealed by the Stern-Gerlach experiment, the discovery of spin might have been significantly delayed. Our findings demonstrate that, even in such scenarios, artificial intelligence can reconstruct the relevant concepts and equations, shedding light on these hidden principles.

Assuming the motion of silver atoms involves only the x -direction, and the direction of the uniform magnetic field is along the z -direction, i.e., $B = B_z \hat{k}$, the Pauli equation describing the motion of silver atoms is:

$$\left[-\frac{\hbar^2}{2m} \frac{d^2}{dx^2} + B_z \mu_B \sigma_z \right] \begin{pmatrix} \psi_1(x) \\ \psi_2(x) \end{pmatrix} = E \begin{pmatrix} \psi_1(x) \\ \psi_2(x) \end{pmatrix}. \quad (37)$$

Similar to the example of the Schrödinger equation, we generate 4000 sets of random potential functions $V_i(x)$ (where $V_i < 0$, $i = 1, 2, \dots, 4000$). The simplified Pauli equation is:

$$\frac{d^2}{dx^2} \begin{pmatrix} \psi_{1i}(x) \\ \psi_{2i}(x) \end{pmatrix} = (V_i(x) \pm B_z) \begin{pmatrix} \psi_{1i}(x) \\ \psi_{2i}(x) \end{pmatrix}, \quad (38)$$

For detailed information about this equation, see Appendix C .

We collect the probability density distribution on the screen as observational data. Since it is a uniform magnetic field, for a given set of random potential functions $V_i(x)$, We have

only a single-component density distribution, corresponding to the single stripe on the screen, which can be expressed as:

$$\rho_i(x) = |\psi_{1i}(x)|^2 + |\psi_{2i}(x)|^2. \quad (39)$$

We initialize both the wave functions $\psi_1(x)$ and $\psi_2(x)$ and their derivatives to 1. Using the previously generated 4,000 sets of potential functions $V_i(x)$ along with the Pauli equation, we produce 4,000 wave function trajectories, each consisting of 100 position steps. By applying Eq.(39), we further compute the corresponding 4,000 probability density trajectories $\rho_i(x)$, which serve as both the input and label for our neural network model. Figure 5(b) displays two sets of random potential functions $V_i(x)$ and their corresponding density distributions $\rho_i(x)$. The differential equations to be discovered are set as:

$$\frac{d\mathbf{h}(x)}{dx} = NN(\mathbf{h}(x), V; \zeta). \quad (40)$$

The results of the ablation experiment shown in Figure 5(c) indicate that the optimal number of physical concepts required to describe this phenomenon is four, suggesting that four variables are necessary to describe this physical system. Similar to the Schrödinger equation case, under the general assumptions of Eq.(40), the network is expected to learn a linear combination of four concepts. Since this multivariable linear combination system is challenging to display graphically, we use the L2 norm of relative errors [100] for validation, with a detailed analysis process described in the Appendix E. The results shown in Figure 5(d) indicate that over an extended period, the relative errors remain very low, demonstrating that all four latent representations have successfully captured the linear combinations of the four variables. Going further, we hope to decouple two differential equations, setting the equations to be discovered as:

$$\frac{d\mathbf{h}_1(x)}{dx} = NN_1(\mathbf{h}_1(x), V; \zeta), \quad (41)$$

$$\frac{d\mathbf{h}_2(x)}{dx} = NN_2(\mathbf{h}_2(x), V; \zeta). \quad (42)$$

Here, $\mathbf{h}_1(x)$ and $\mathbf{h}_2(x)$ are two-component vectors. Each component means a latent representation. After training, as shown in Figure 5(e), we find that the first two latent representations store the linear combination of ψ_1 and $\dot{\psi}_1$, and the other ones store a linear combination of ψ_2 and $\dot{\psi}_2$. This indicates that the neural network are capable of distinguishing and representing the spin components of the system. Then we unravel these linear combinations by setting the differential equations to be second-order:

$$\frac{dh_{11}(x)}{dx} = h_{12}(x), \quad \frac{dh_{12}(x)}{dx} = NN_1(h_{11}(x), h_{12}(x), V; \zeta). \quad (43)$$

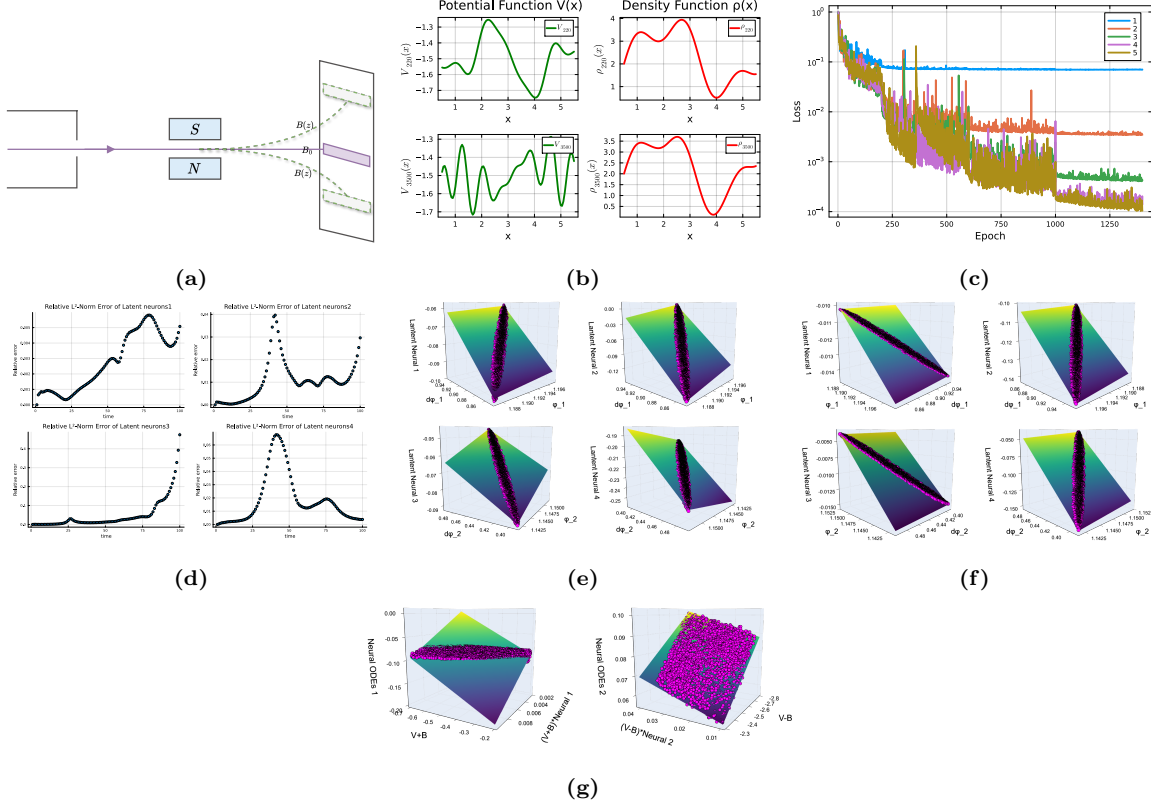


Figure 5: The Pauli Equation Model. (a) Schematic of Stern-Gerlach experiment under a uniform magnetic field (pink) and non-uniform magnetic field (green). (b) Random potentials (green) and corresponding density distributions (red). (c) Impact of latent dimensions on loss, showing a four-dimensional space as optimal. (d) L2 norm of relative errors between neural outputs and predictions. (e) Latent representations with first-order differential equations: first two neurons store linear combinations of ψ_1 and $\dot{\psi}_1$; the other two store linear combinations of ψ_2 and $\dot{\psi}_2$. (f) Latent representations with second-order differential equations: neurons separately capture ψ_1 , $\dot{\psi}_1$, ψ_2 , and $\dot{\psi}_2$. (g) Successful learning of two second-order differential equations by Neural ODEs.

$$\frac{dh_{21}(x)}{dx} = h_{22}(x), \quad \frac{dh_{22}(x)}{dx} = NN_2(h_{21}(x), h_{22}(x), V; \zeta). \quad (44)$$

Figure 5(f) shows that after training, the four latent representations each independently store ψ_1 , $\dot{\psi}_1$, ψ_2 , and $\dot{\psi}_2$ (differing only by a scaling transformation).

This demonstrates that the neural network not only successfully differentiates between the two spin-1/2 components (ψ_1 and ψ_2) but also captures their dynamics ($\dot{\psi}_1$ and $\dot{\psi}_2$). The four representations h_{11} , h_{12} , h_{21} and h_{22} have captured the underlying concepts, differing only by a linear transformation:

$$h_{11} = a_1 \cdot \psi_1 + b_1, \quad (45)$$

$$h_{12} = a_2 \cdot \frac{d\psi_1}{dx} + b_2, \quad (46)$$

$$h_{21} = a_3 \cdot \psi_2 + b_3, \quad (47)$$

$$h_{22} = a_4 \cdot \frac{d\psi_2}{dx} + b_4. \quad (48)$$

we can further obtain:

$$NN_1 = \frac{dh_{12}}{dx} = \frac{a_2}{a_1} \cdot [(V + B_z) \cdot h_{11}] - \frac{a_2 \cdot b_1}{a_1} \cdot (V + B_z), \quad (49)$$

$$NN_2 = \frac{dh_{22}}{dx} = \frac{a_4}{a_3} \cdot [(V - B_z) \cdot h_{21}] - \frac{a_4 \cdot b_3}{a_3} \cdot (V - B_z). \quad (50)$$

These two equations are exactly what Neural ODEs have learned, as shown in Figure 5(g). The left plot corresponds to the learned output NN_1 by Neural ODEs (z-axis) plotted against the variables $(V + B_z) \cdot h_{11}$ (x-axis) and $(V + B_z)$ (y-axis). The right plot represents the learned output NN_2 (z-axis) against the variables $(V - B_z) \cdot h_{21}$ (x-axis) and $(V - B_z)$ (y-axis). Both plots clearly reveal a linear relationship among these variables, indicating that Neural ODEs have effectively captured the underlying dynamical equations in both cases.

4 Conclusion and discussion

4.1 Conclusion

In this study, we extend the model introduced in *SciNet*, which leverages machine learning to identify physical concepts and aims to emulate human physical reasoning. Building upon *SciNet*'s questioning mechanism, we integrate Variational Autoencoders and Neural Ordinary Differential Equations to propose a neural network framework capable of simultaneously discovering physical concepts and governing equations. The feasibility and broad applicability of this framework are demonstrated through four significant case studies, ranging from classical to quantum physics.

One particularly notable case involves the investigation of spin-1/2 particles and the Pauli equation. Our study highlights an intriguing difference from the historical development of physics. Traditionally, physicists developed the theory by interpreting the two distinct stripes observed in the Stern-Gerlach experiment under a non-uniform magnetic field, combining experimental observations with theoretical reasoning. In contrast, our research shows that an end-to-end approach enables a machine to directly extract latent physical patterns from experimental data obtained under a uniform magnetic field, where only a single stripe is observed, ultimately reconstructing the same physical theory.

Looking ahead, we plan to extend the model’s capabilities from discovering ordinary differential equations to partial differential equations, enabling the exploration of more fundamental physical theories such as the time-dependent Schrödinger equation and the Dirac equation in four-dimensional spacetime.

As a proof-of-principle, this study showcases the potential of machine learning to derive physical theories directly from data, reducing traditional reliance on prior physical knowledge. By aligning theoretical models with experimental results in a fully data-driven manner, we aim to establish foundational AI models for theoretical physics, providing novel tools for uncovering new physical insights.

4.2 Discussion

Our approach is capable of automatically discovering physical concepts and governing equations, but it also faces certain limitations in its application. For instance, in the case of Newton’s law of universal gravitation, the performance of the neural network deteriorates as the range of evolution time in the observational data increases. We speculate that this may be due to the growing differences among trajectories over extended time periods, which increase the complexity of the data and hinder the model’s ability to effectively learn the underlying physical laws. Similarly, in the case of spin-1/2 particles with the Pauli equation, the neural network performs better on data corresponding to earlier step points compared to its performance on data from later step points.

These challenges can be attributed to the inherent “curse of length” problem in Neural ODEs [101–103], which limits their ability to effectively learn and generalize physical laws over longer time scales. Several potential approaches can be explored in the future to address this issue. For example, Iakovlev et al. [102] proposed using sparse Bayesian multiple shooting techniques integrated with Transformers within Neural ODEs models. This approach segments longer trajectories into shorter fragments and optimizes them in parallel, thereby improving efficiency and stability.

Despite these technical challenges, our study demonstrates that a machine learning framework combining the joint training of physical concept identification and equation discovery modules, along with the integration of a questioning mechanism and universal constraints, can successfully uncover hidden physical theories. Future improvements to this framework can be pursued in several directions. For instance, employing more powerful machine learning models than VAEs and Neural ODEs to learn physical concepts and equations; designing more effective questioning mechanisms to guide the learning process;

integrating multi-faceted constraints from physics, mathematics, and machine learning; and incorporating symbolic regression to enhance both the interpretability of the framework and the accuracy of the discovered physical theories.

Acknowledgments

We thank Sven Krippendorf and Yukun Yan for their valuable discussion.

A Analytical Derivation of the Loss Function

Our model’s loss function consists of two components: the reconstruction loss L_R and the regularization loss L_{KL} . We introduce a hyperparameter β to balance the trade-off between encouraging the independence of the latent variables and controlling the regularization strength. Additionally, we account for the parameters ζ of Neural ODEs network. The overall loss function is then defined as:

$$L(\mathbf{x}; \phi, \zeta, \theta) = L_R(\mathbf{x}; \phi, \zeta, \theta) + \beta \cdot L_{KL}(\mathbf{x}; \phi, \zeta, \theta), \quad (\text{A.1})$$

where

$$L_R(\mathbf{x}; \phi, \zeta, \theta) = -\mathbb{E}_{q_\phi(\mathbf{z}|\mathbf{x})}[\log p_\theta(\mathbf{x}|\mathbf{z})], \quad (\text{A.2})$$

$$L_{KL}(\mathbf{x}; \phi, \zeta, \theta) = D_{KL}(q_\phi(\mathbf{z}|\mathbf{x})||p_\theta(\mathbf{z})). \quad (\text{A.3})$$

First, we address the reconstruction error $L_R(\mathbf{x}; \phi, \zeta, \theta)$. For a given set of data x^i , assume the decoder $p_\theta(x^i|z^i)$ outputs a conditional probability distribution as a Gaussian, where the decoder’s output $\hat{x}^i = f_\theta(z^i)$ is the mean of the Gaussian distribution with a variance of 1. This implies that for each data point in a given set x^i , such as $x_1^i, x_2^i, \dots, x_k^i$, we have:

$$p_\theta(x^i|z^i) = \frac{1}{\sigma^i \sqrt{2\pi}} \exp\left(-\frac{(x^i - \hat{x}^i)^2}{2}\right), \quad (\text{A.4})$$

Based on the form of reconstruction error Eq.(A.2), we have:

$$L_R(x^i; \phi, \zeta, \theta) = -\mathbb{E}_{q_\phi(z^i|x^i)}\left[-\frac{1}{2}(x^i - \hat{x}^i)^2 + \log \frac{1}{\sqrt{2\pi}}\right], \quad (\text{A.5})$$

Here, $\mathbb{E}_{q_\phi(z^i|x^i)}$ represents the expectation over a function of the latent variable z^i under the probability distribution $q_\phi(z^i|x^i)$, determined by parameter ϕ , given the input x^i . Since direct computation of this expectation is challenging, we may use the Monte Carlo approximation by sampling k instances $z_1^i, z_2^i, \dots, z_k^i$ from $q_\phi(z^i|x^i)$, and approximate this expectation by the sample average:

$$L_R(x^i; \phi, \zeta, \theta) \approx \frac{1}{k} \sum_{l=1}^k \left[\frac{1}{2}(x_l^i - \hat{x}_l^i)^2\right] + \text{const}, \quad (\text{A.6})$$

In the optimization process, the constant term in the loss function Eq.(A.6) does not affect the overall optimization, so the reconstruction error for the i -th data set x^i is further expressed as:

$$L_R(x^i; \phi, \zeta, \theta) = \frac{1}{k} \sum_{l=1}^k [(x_l^i - \hat{x}_l^i)^2]. \quad (\text{A.7})$$

Next, we address the regularization loss $L_{KL}(\mathbf{x}; \phi, \zeta, \theta)$. In our network architecture, the Encoder neural network models the posterior probability distribution $q_\phi(\mathbf{z}|\mathbf{x})$, which we assume to follow a multivariate Gaussian distribution: $q_\phi(\mathbf{z}|\mathbf{x}) = \mathcal{N}(\mathbf{z}; \boldsymbol{\mu}, \boldsymbol{\sigma}^2 I)$, where $\boldsymbol{\mu}$ and $\boldsymbol{\sigma}^2$ are the mean and variance of the latent variable \mathbf{z} , output by the Encoder network. We assume the prior distribution $p_\theta(\mathbf{z})$ to be a standard multivariate Gaussian: $p_\theta(\mathbf{z}) = \mathcal{N}(\mathbf{z}; 0, I)$, where the mean is zero and the variance is the identity matrix I (of dimension D).

For a given set of data x^i , the probability density function of a multivariate Gaussian distribution is:

$$p(x^i) = p(x_1^i, x_2^i, \dots, x_D^i) = \prod_{d=1}^D p(x_d^i) = \prod_{d=1}^D \frac{1}{\sqrt{2\pi}\sigma_d^i} \exp\left(-\frac{(x_d^i - \mu_d^i)^2}{2\sigma_d^i}\right), \quad (\text{A.8})$$

Thus, we have:

$$q_\phi(z^i | x^i) = \mathcal{N}(z^i; \mu^i, \sigma^{i^2} I) = \prod_{d=1}^D \frac{1}{\sqrt{2\pi}\sigma_d^i} \exp\left(-\frac{(z_d^i - \mu_d^i)^2}{2\sigma_d^i}\right), \quad (\text{A.9})$$

$$p_\theta(z^i) = \mathcal{N}(z^i; 0, I) = \prod_{d=1}^D \frac{1}{\sqrt{2\pi}} \exp\left(-\frac{z_d^i{}^2}{2}\right), \quad (\text{A.10})$$

Here, z_d^i , μ_d^i , and σ_d^i are the d -th elements of the vectors z^i , μ^i , and σ^i for the i -th data set.

The definition of Kullback-Leibler divergence $D_{KL}(q_\phi(z^i|x^i)||p_\theta(z^i))$ is:

$$\begin{aligned} D_{KL}(q_\phi(z^i | x^i) | p_\theta(z^i)) &= \int q_\phi(z^i|x^i) \log\left(\frac{q_\phi(z^i|x^i)}{p_\theta(z^i)}\right) dz^i \\ &= \mathbb{E}_{q_\phi(z^i|x^i)}[\log q_\phi(z^i|x^i)] - \mathbb{E}_{q_\phi(z^i|x^i)}[\log p_\theta(z^i)], \end{aligned} \quad (\text{A.11})$$

Substituting Eq.(A.9) and Eq.(A.10) into Eq.(A.11), we have:

$$\mathbb{E}_{q_\phi(z^i|x^i)} \log q_\phi(z^i | x^i) = \frac{1}{2} \sum_{d=1}^D \left(-\log 2\pi - \log \sigma_d^i - 1\right), \quad (\text{A.12})$$

$$\mathbb{E}_{q_\phi(z^i|x^i)} [\log p_\theta(z^i)] = \frac{1}{2} \sum_{d=1}^D \left(-\log 2\pi - \mu_d^i{}^2 - \sigma_d^i\right), \quad (\text{A.13})$$

Substituting Eq.(A.12) and Eq.(A.13) into Eq.(A.11), the analytical expression for KL divergence D_{KL} is:

$$D_{KL}(q_\phi(z^i | x^i) | p_\theta(z^i)) = \frac{1}{2} \sum_{d=1}^D \left(\mu_d^i{}^2 + \sigma_d^i - \log \sigma_d^i - 1\right). \quad (\text{A.14})$$

Substituting the reconstruction error Eq.(A.7) and KL divergence Eq.(A.14) into the loss function Eq.(A.1), we have:

$$L(\mathbf{x}; \phi, \zeta, \theta) = \frac{1}{N} \sum_{i=1}^N \left[\frac{1}{k} \sum_{l=1}^k [(x_l^i - \hat{x}_l^i)^2] + \frac{\beta}{2} \sum_{d=1}^D (\mu_d^{i^2} + \sigma_d^{i^2} - \log \sigma_d^{i^2} - 1) \right]. \quad (\text{A.15})$$

Eq.(A.15) is the specific numerical form of our neural network’s loss function, where D represents the dimensionality of the latent space. In our experimental process, the most appropriate values will be determined through ablation studies.

B Random Potential

Random potential functions play a significant role in the study of physics, extensively used to investigate the diffusion movement of electrons in disordered lattices [104, 105]. In the study of Anderson localization [104], by introducing random potential functions, one can construct the Hamiltonian of electrons in disordered systems to study the phenomenon of electron localization. Additionally, random potential functions are used to describe the random distribution of impurities in materials [106–108]. The random collisions between impurities and electrons lead to changes in the behavior of electron gas. By incorporating random potential functions into the Hamiltonian of electron gas, a more realistic theoretical model can be established.

In this article, the generation process for the random potential function $V_i(x)$ we use is as follows:

1. Base Functions: Define a set of base functions:

$$f(x) = \{\sin(jx) | j = 1, 2, \dots, 9\}, \quad (\text{B.1})$$

2. Random Coefficients: In each iteration, generate a set of random coefficients:

$$v_{\text{coef}} = [c_1, \dots, c_j, \dots, c_9], \quad (\text{B.2})$$

where c_j is drawn from a standard normal distribution (Gaussian with mean 0 and variance 1).

3. Constructing Random Potential:

$$v(x) = \sum_{j=1}^9 c_j \sin(jx) - 1, \quad (\text{B.3})$$

4. Condition Verification: Verify if the random potential function satisfies the condition within the testing range:

$$-3 < v(x) < 0, \quad \forall x \in x_{\text{test}}, \quad (\text{B.4})$$

5. **Collecting Coefficients:** If the random potential function satisfies the above conditions, collect the corresponding coefficients into a specified set. This process continues until N sets of satisfying coefficients are collected:

$$[v_{\text{coef}}^1, v_{\text{coef}}^2, \dots, v_{\text{coef}}^i, \dots, v_{\text{coef}}^N], \quad (\text{B.5})$$

where $v_{\text{coef}}^i = [c_1^i, \dots, c_j^i, \dots, c_9^i]$.

6. **Calculating the Final Potential Function:** Use the collected N sets of coefficients to calculate the final set of N potential functions. The random potential functions for the Schrödinger equation and the Pauli equation are respectively:

$$V_i(x) = \sum_{j=1}^9 c_j^i \sin(jx) - 1, \quad V_i(x) = \frac{\sum_{j=1}^9 c_j^i \sin(jx) - 6}{4}. \quad (\text{B.6})$$

where $V_i(x)$ is one of the N sets of potential functions. In the case of the Pauli equation, we selected an appropriate range for the potential function to ensure that the two generated wave functions have a certain degree of distinction, making them easier to differentiate, while avoiding excessive differences that would significantly increase the learning difficulty.

This structured approach allows the neural network to incorporate physical characteristics modeled by random potential, further enhancing its ability to simulate and understand complex physical phenomena.

C Motion in the Stern-Gerlach Experiment in Non-uniform and Uniform Magnetic Fields

In this section, we begin with the results of the Stern-Gerlach experiment in a non-uniform magnetic field and extend our analysis to the case of a uniform magnetic field, leading to the Pauli equation that describes this process.

In the Stern-Gerlach experiment, the spin of silver atoms causes a beam passing through a non-uniform magnetic field to split into two distinct directions, producing two symmetric stripes on a screen, as indicated by the dashed lines in Figure 5(a). For a spin-1/2 system with motion along the x -direction and a non-uniform magnetic field $B(z)$ along the z -direction, and no motion in the y -direction, the system's Hamiltonian H is given by:

$$H = \frac{p_x^2}{2m} + \frac{p_z^2}{2m} + B(z)\mu_B\sigma_z. \quad (\text{C.1})$$

where $B(z)\mu_B\sigma_z$ is the energy term due to the interaction of the magnetic moment of silver atoms with the external magnetic field $B(z)$, commonly referred to as the spin-magnetic field interaction term.

The motion of silver atoms can be described by the Pauli equation:

$$i\hbar \frac{\partial}{\partial t} \Psi(x, z, t) = H \Psi(x, z, t), \quad (\text{C.2})$$

where $\Psi(x, z, t)$ is a two-component wave function, expressed as:

$$\Psi(x, z, t) = \begin{bmatrix} \Psi_1(x, z, t) \\ \Psi_2(x, z, t) \end{bmatrix}, \quad (\text{C.3})$$

$\Psi_1(x, z, t)$ represents the spin-up state, and $\Psi_2(x, z, t)$ represents the spin-down state.

Thus, the motion equation for silver atoms in a non-uniform magnetic field describing the Stern-Gerlach experiment is:

$$i\hbar \frac{\partial}{\partial t} \begin{bmatrix} \Psi_1(x, z, t) \\ \Psi_2(x, z, t) \end{bmatrix} = \left(\frac{p_x^2}{2m} + \frac{p_z^2}{2m} \pm B(z)\mu_B\sigma_z \right) \begin{bmatrix} \Psi_1(x, z, t) \\ \Psi_2(x, z, t) \end{bmatrix}. \quad (\text{C.4})$$

We extend the Stern-Gerlach experiment to a uniform magnetic field. In this case, the beam of silver atoms passing through a uniform magnetic field does not split into two stripes as in a non-uniform magnetic field but leaves a single stripe on the screen, as shown by the solid line in Figure 5(a). In this scenario, the spin and other related physical principles are hidden within this single stripe.

Assuming the motion of silver atoms involves only the x -direction, and the direction of the uniform magnetic field is along the z -direction, i.e., $B = B_z \hat{k}$. The system's Hamiltonian H can be represented as:

$$H = \frac{p_x^2}{2m} + B_z \mu_B \sigma_z. \quad (\text{C.5})$$

Therefore, the motion equation for silver atoms in the Stern-Gerlach experiment under a uniform magnetic field B_z is:

$$i\hbar \frac{\partial}{\partial t} \begin{bmatrix} \Psi_1(x, t) \\ \Psi_2(x, t) \end{bmatrix} = \left(\frac{p_x^2}{2m} \pm B_z \mu_B \sigma_z \right) \begin{bmatrix} \Psi_1(x, t) \\ \Psi_2(x, t) \end{bmatrix}, \quad (\text{C.6})$$

After separating variables in the wave function, we have:

$$\begin{bmatrix} \Psi_1(x, t) \\ \Psi_2(x, t) \end{bmatrix} = \begin{bmatrix} \psi_1(x) \\ \psi_2(x) \end{bmatrix} \phi(t), \quad (\text{C.7})$$

Solving Eq.(C.6) yields the stationary Pauli equation for silver atoms:

$$-\frac{\hbar^2}{2m} \frac{d^2}{dx^2} \psi_1(x) = (E + B_z \mu_B) \psi_1(x), \quad (\text{C.8})$$

$$-\frac{\hbar^2}{2m} \frac{d^2}{dx^2} \psi_2(x) = (E - B_z \mu_B) \psi_2(x). \quad (\text{C.9})$$

To simplify these equations and make them more suitable for simulation and learning through neural networks, we simplify Eq.(C.8) and Eq.(C.9) formally. First, multiplying both sides of Eq.(C.8) and Eq.(C.9) by $-2m/\hbar^2$ eliminates the constant coefficient on the left side of the equations, resulting in:

$$\frac{d^2}{dx^2}\psi_1(x) = -\frac{2m}{\hbar^2}(E + B_z\mu_B)\psi_1(x), \quad (\text{C.10})$$

$$\frac{d^2}{dx^2}\psi_2(x) = -\frac{2m}{\hbar^2}(E - B_z\mu_B)\psi_2(x). \quad (\text{C.11})$$

Next, to further simplify these equations, we introduce 4000 sets of random potential functions $V_i(x)$ ($i=1,2,\dots,4000$), ensuring $V_i < 0$, to keep the particles in an extended state, similar to the Schrödinger equation where the potential energy is always measured relative to the particle’s energy, thereby fixing the particle’s energy at zero. We define:

$$B = B_z\mu_B. \quad (\text{C.12})$$

The simplified component form of the Pauli equation can be obtained:

$$\frac{d^2}{dx^2}\psi_1(x) = (V(x) + B)\psi_1(x), \quad (\text{C.13})$$

$$\frac{d^2}{dx^2}\psi_2(x) = (V(x) - B)\psi_2(x). \quad (\text{C.14})$$

Here, $V(x)$ is a random potential function Eq.(B.6), and $B = 1.05$ is a constant magnetic field. To keep the particles in an extended state, we need to ensure that both $V(x) + B$ and $V(x) - B$ are less than zero.

Through the derivation outlined above, we have successfully simplified the Pauli equation describing the motion of silver atoms in a uniform magnetic field during the Stern-Gerlach experiment. By introducing a random potential function $V(x)$ and assuming that the particle energy is fixed at zero, we have made the equation more suitable for learning and simulation using neural networks. This approach not only preserves the core characteristics of the physical system but also optimizes the structure of the equation, making it easier to handle and compute.

D Network Details and Training Process

D.1 Network Details

The model architecture consists of three core components: the Encoder, the Neural ODEs layer, and the Decoder. The specific implementation details of these three parts may vary

across different application cases. To illustrate these differences, we have listed the detailed information and the activation functions used for each network part in Table 1.

Table 1: Network structure parameters.

Example	Input Size	Latent Neurons	Output Size	E(D)ncoder	NODE Input	NODE Output	NODE
Heliocentric	2	2	2	(30, 30, tanh)	3	1	(16, 16, tanh)
Gravitational	1	2	1	(64, 64, relu)	3	2	(16, 16, tanh)
Gravitational (2nd Ord)	1	2	1	(64, 64, relu)	3	1	(16, 16, tanh)
Sch. Eq.	50	2	1	(64, 64, relu)	3	2	(16, 16, tanh)
Sch. Eq. (2nd Ord)	50	2	1	(64, 64, relu)	3	1	(16, 16, tanh)
Pauli Eq. (1 NODE)	100	4	1	(64, 64, relu)	5	4	(16, 16, tanh)
Pauli Eq.	100	4	1	(64, 64, relu)	3 3	2 2	(16, 16, tanh)
Pauli Eq. (2nd Ord)	100	4	1	(64, 64, relu)	3 3	1 1	(16, 16, tanh)

The Encoder, Neural ODEs, and Decoder are all fully connected neural networks. Our Neural ODEs are solved using the Tsitouras 5/4 Runge-Kutta method [109].

D.2 Training Process

During the training process, neural network parameters (ϕ, ζ, θ) , where ϕ , ζ , and θ are parameters of the Encoder, Neural ODEs, and Decoder respectively, are optimized using the RMSProp optimizer, Adam optimizer, and BFGS optimizer. For different application cases, learning rates, the hyperparameter β , and the number of training epochs vary, as specified in Table 2.

In all cases, we use Kaiming initialization [110] to initialize the network parameters. The key idea behind Kaiming initialization is to consider the variance of weight gradients during forward and backward propagation when initializing weights in each layer of the network, thereby preventing gradient vanishing or explosion and ensuring stable learning of the network.

Table 2: Parameters During the Training Process

Example	Learning Rate	β	Epoch/MaxIter
Heliocentric	0.01-0.0001	0.01	3000
Gravitation	0.01-0.001	0	2200
Gravitational (2nd Ord)	0.01-0.001	0	2200
Sch. Eq.	0.01-0.001	0.001	1600
Sch. Eq. (2nd Ord)	0.01-0.001	0.001	1600
Pauli Eq. (1 NODE)	0.01-0.001	0.0001	2600
Pauli Eq.	0.01-0.001	0.0001	1400
Pauli Eq. (2nd Ord)	0.01-0.0001	0.1	1400

During the training, by fixing β , adjusting the learning rate and the number of training iterations, the loss is minimized. The entire training process is divided into three stages:

1. In this phase, we use the RMSProp optimizer, which adjusts the learning rate dynamically and is well-suited for non-stationary objectives, making it effective for a variety of common deep learning problems. We set the learning rate to 0.005 and limit the number of iterations to 200. This phase helps to screen multiple sets of effective training parameters.

2. Large-Scale Training Phase: Following preliminary screening, we switch to the Adam optimizer for more extensive training iterations. Adam combines the advantages of both RMSProp and Momentum optimizers, adjusting learning rates based on estimates of the first-order (momentum) and second-order moments of gradients, enabling more refined parameter adjustments. For all cases, the initial learning rate is set to 0.01, followed by a gradual reduction after a predefined number of epochs.

3. Fine-Tuning Parameters Phase: Finally, we apply the BFGS (Broyden-Fletcher-Goldfarb-Shanno) optimizer for small-batch training using the best set of parameters identified in the previous phase. As a quasi-Newton method, BFGS optimizes the loss function by approximating second-order derivatives (the Hessian matrix). The goal of this phase is to precisely find the global minimum of the loss function based on the parameters already optimized.

E Multivariable Linear System Analysis

In the case of the Pauli equation, we determined through ablation experiments that the optimal number of physical concepts describing the system is four. By analyzing the case of the Schrödinger equation, we predict that the neural network will learn a linear combination of these four variables. Since directly displaying a multivariable linear system graphically is complex, we proceed with the verification through the following steps:

1. We represent the output of each neuron in the neural network, $\mathbf{N}(k, \mathbf{x})$, as a linear combination of four known real vector variables: $\psi_1(\mathbf{x})$, $d\psi_1(\mathbf{x})/d\mathbf{x}$, $\psi_2(\mathbf{x})$, $d\psi_2(\mathbf{x})/d\mathbf{x}$. The specific formula is:

$$\mathbf{N}(k, \mathbf{x}) = a \cdot \psi_1(\mathbf{x}) + b \cdot \frac{d\psi_1(\mathbf{x})}{d\mathbf{x}} + c \cdot \psi_2(\mathbf{x}) + d \cdot \frac{d\psi_2(\mathbf{x})}{d\mathbf{x}} + \text{const}, \quad (\text{E.1})$$

where $k = 1, 2, 3, 4$ corresponds to the outputs of the four neurons.

2. By fitting, we obtain the linear coefficients a , b , c , d , and constant. We use these coefficients to calculate the predicted output for 4000 sample points:

$$\text{Predict}_i(x) = a \cdot \psi_{1_i}(x) + b \cdot \frac{d\psi_{1_i}(x)}{dx} + c \cdot \psi_{2_i}(x) + d \cdot \frac{d\psi_{2_i}(x)}{dx} + \text{const}, \quad (\text{E.2})$$

3. We evaluate the model performance by calculating the $L2$ norm of the relative error [100] between $\mathbf{N}(k, \mathbf{x})$ and the predicted output $\mathbf{Predict}(\mathbf{x})$:

$$\frac{\|\mathbf{N}(\mathbf{k}, \mathbf{x}) - \mathbf{Predict}(\mathbf{x})\|_2}{\|\mathbf{N}(\mathbf{k}, \mathbf{x})\|_2}. \quad (\text{E.3})$$

4. We analyze this error. If the error is minimal, it indicates that the neurons have indeed learned the linear combination of these four variables.

References

- [1] Einstein, A. On the method of theoretical physics. *Philosophy Of Science*. **1**, 163-169 (1934)
- [2] Maillet, J. Heisenberg spin chains: from quantum groups to neutron scattering experiments. *Quantum Spaces*. pp. 161-201 (2007)
- [3] Yu, R. & Wang, R. Learning dynamical systems from data: An introduction to physics-guided deep learning. *Proceedings Of The National Academy Of Sciences*. **121**, e2311808121 (2024)
- [4] Zhang, X., Wang, L., Helwig, J., Luo, Y., Fu, C., Xie, Y., Liu, M., Lin, Y., Xu, Z., Yan, K. & Others Artificial intelligence for science in quantum, atomistic, and continuum systems. *ArXiv Preprint [arXiv:2307.08423](https://arxiv.org/abs/2307.08423)*. (2023)
- [5] Wang, H., Fu, T., Du, Y., Gao, W., Huang, K., Liu, Z., Chandak, P., Liu, S., Van Katwyk, P., Deac, A. & Others Scientific discovery in the age of artificial intelligence. *Nature*. **620**, 47-60 (2023)
- [6] Lucie-Smith, L., Peiris, H., Pontzen, A., Nord, B., Thiyagalingam, J. & Piras, D. Discovering the building blocks of dark matter halo density profiles with neural networks. *Physical Review D*. **105**, 103533 (2022)
- [7] Övgün, A., Sakallı, İ. & Mutuk, H. Quasinormal modes of dS and AdS black holes: Feedforward neural network method. *International Journal Of Geometric Methods In Modern Physics*. **18**, 2150154 (2021)
- [8] Ravanbakhsh, S., Oliva, J., Fromenteau, S., Price, L., Ho, S., Schneider, J. & Póczos, B. Estimating cosmological parameters from the dark matter distribution. *International Conference On Machine Learning*. pp. 2407-2416 (2016)
- [9] Zhang, X., Wang, Y., Zhang, W., Sun, Y., He, S., Contardo, G., Villaescusa-Navarro, F. & Ho, S. From dark matter to galaxies with convolutional networks. *ArXiv Preprint [arXiv:1902.05965](https://arxiv.org/abs/1902.05965)*. (2019)
- [10] Peel, A., Lalande, F., Starck, J., Pettorino, V., Merten, J., Giocoli, C., Meneghetti, M. & Baldi, M. Distinguishing standard and modified gravity cosmologies with machine learning. *Physical Review D*. **100**, 023508 (2019)

- [11] Ntampaka, M., ZuHone, J., Eisenstein, D., Nagai, D., Vikhlinin, A., Hernquist, L., Marinacci, F., Nelson, D., Pakmor, R., Pillepich, A. & Others A deep learning approach to galaxy cluster x-ray masses. *The Astrophysical Journal*. **876**, 82 (2019)
- [12] Krippendorf, S., Perez, N., Bulbul, E., Kara, M., Seppi, R., Comparat, J., Artis, E., Bahar, Y., Garrel, C., Ghirardini, V. & Others The eROSITA Final Equatorial-Depth Survey (eFEDS): A machine learning approach to inferring galaxy cluster masses from eROSITA X-ray images. *Astronomy & Astrophysics*. **682** pp. A132 (2024)
- [13] Yan, Y., Wu, S., Ge, X. & Tian, Y. Deep learning black hole metrics from shear viscosity. *Physical Review D*. **102**, 101902 (2020)
- [14] Villaescusa-Navarro, F., Anglés-Alcázar, D., Genel, S., Spergel, D., Somerville, R., Dave, R., Pillepich, A., Hernquist, L., Nelson, D., Torrey, P. & Others The camels project: Cosmology and astrophysics with machine-learning simulations. *The Astrophysical Journal*. **915**, 71 (2021)
- [15] Akutagawa, T., Hashimoto, K. & Sumimoto, T. Deep learning and AdS/QCD. *Physical Review D*. **102**, 026020 (2020)
- [16] Hashimoto, K., Sugishita, S., Tanaka, A. & Tomiya, A. Deep learning and the AdS/CFT correspondence. *Physical Review D*. **98**, 046019 (2018)
- [17] Karagiorgi, G., Kasieczka, G., Kravitz, S., Nachman, B. & Shih, D. Machine learning in the search for new fundamental physics. *Nature Reviews Physics*. **4**, 399-412 (2022)
- [18] Albertsson, K., Altoe, P., Anderson, D., Andrews, M., Araque Espinosa, J., Aurisano, A., Basara, L., Bevan, A., Bhimji, W., Bonacorsi, D. & Others Machine learning in high energy physics community white paper. *Journal Of Physics: Conference Series*. **1085** pp. 022008 (2018)
- [19] Guest, D., Cranmer, K. & Whiteson, D. Deep learning and its application to LHC physics. *Annual Review Of Nuclear And Particle Science*. **68**, 161-181 (2018)
- [20] Guan, W., Perdue, G., Pesah, A., Schuld, M., Terashi, K., Vallecorsa, S. & Vlimant, J. Quantum machine learning in high energy physics. *Machine Learning: Science And Technology*. **2**, 011003 (2021)

- [21] Arsenault, L., Lopez-Bezanilla, A., Von Lilienfeld, O. & Millis, A. Machine learning for many-body physics: The case of the Anderson impurity model. *Physical Review B*. **90**, 155136 (2014)
- [22] Kumar, P., Mandal, T. & Mondal, S. Black Holes and the loss landscape in machine learning. *Journal Of High Energy Physics*. **2023**, 1-31 (2023)
- [23] Choi, E. & Seong, R. Machine learning regularization for the minimum volume formula of toric Calabi-Yau 3-folds. *Physical Review D*. **109**, 046015 (2024)
- [24] Ruehle, F. Evolving neural networks with genetic algorithms to study the String Landscape. *Journal Of High Energy Physics*. **2017**, 1-20 (2017)
- [25] Deen, R., He, Y., Lee, S. & Lukas, A. Machine learning string standard models. *Physical Review D*. **105**, 046001 (2022)
- [26] Gao, X. & Zou, H. Applying machine learning to the Calabi-Yau orientifolds with string vacua. *Physical Review D*. **105**, 046017 (2022)
- [27] Cao, Z., Luo, X., Lv, J. & Wang, L. Space Group Informed Transformer for Crystalline Materials Generation. *ArXiv Preprint [arXiv:2403.15734](https://arxiv.org/abs/2403.15734)*. (2024)
- [28] Carrasquilla, J. & Melko, R. Machine learning phases of matter. *Nature Physics*. **13**, 431-434 (2017)
- [29] Carleo, G. & Troyer, M. Solving the quantum many-body problem with artificial neural networks. *Science*. **355**, 602-606 (2017)
- [30] Bernien, H., Schwartz, S., Keesling, A., Levine, H., Omran, A., Pichler, H., Choi, S., Zibrov, A., Endres, M., Greiner, M. & Others Probing many-body dynamics on a 51-atom quantum simulator. *Nature*. **551**, 579-584 (2017)
- [31] Zhang, J., Pagano, G., Hess, P., Kyprianidis, A., Becker, P., Kaplan, H., Gorshkov, A., Gong, Z. & Monroe, C. Observation of a many-body dynamical phase transition with a 53-qubit quantum simulator. *Nature*. **551**, 601-604 (2017)
- [32] Chen, B., Huang, K., Raghupathi, S., Chandratreya, I., Du, Q. & Lipson, H. Automated discovery of fundamental variables hidden in experimental data. *Nature Computational Science*. **2**, 433-442 (2022)

- [33] Camps-Valls, G., Gerhardus, A., Ninad, U., Varando, G., Martius, G., Balaguer-Ballester, E., Vinuesa, R., Diaz, E., Zanna, L. & Runge, J. Discovering causal relations and equations from data. *Physics Reports*. **1044** pp. 1-68 (2023)
- [34] Brunton, S., Proctor, J. & Kutz, J. Discovering governing equations from data by sparse identification of nonlinear dynamical systems. *Proceedings Of The National Academy Of Sciences*. **113**, 3932-3937 (2016)
- [35] Champion, K., Lusch, B., Kutz, J. & Brunton, S. Data-driven discovery of coordinates and governing equations. *Proceedings Of The National Academy Of Sciences*. **116**, 22445-22451 (2019)
- [36] Wu, T. & Tegmark, M. Toward an artificial intelligence physicist for unsupervised learning. *Physical Review E*. **100**, 033311 (2019)
- [37] Zhang, Z. & You, Y. Observing Schrödinger’s cat with artificial intelligence: emergent classicality from information bottleneck. *Machine Learning: Science And Technology*. **5**, 015051 (2024)
- [38] Raissi, M. & Karniadakis, G. Hidden physics models: Machine learning of nonlinear partial differential equations. *Journal Of Computational Physics*. **357** pp. 125-141 (2018)
- [39] Wang, C., Zhai, H. & You, Y. Emergent Schrödinger equation in an introspective machine learning architecture. *Science Bulletin*. **64**, 1228-1233 (2019)
- [40] Iten, R., Metger, T., Wilming, H., Del Rio, L. & Renner, R. Discovering physical concepts with neural networks. *Physical Review Letters*. **124**, 010508 (2020)
- [41] Desai, K., Nachman, B. & Thaler, J. Symmetry discovery with deep learning. *Physical Review D*. **105**, 096031 (2022)
- [42] Otto, S., Zolman, N., Kutz, J. & Brunton, S. A unified framework to enforce, discover, and promote symmetry in machine learning. *ArXiv Preprint [arXiv:2311.00212](https://arxiv.org/abs/2311.00212)*. (2023)
- [43] Cory-Wright, R., El Khadir, B., Cornelio, C., Dash, S. & Horesh, L. AI Hilbert: a new paradigm for scientific discovery by unifying data and background knowledge. *ArXiv Preprint [arXiv:2308.09474](https://arxiv.org/abs/2308.09474)*.

- [44] Lemos, P., Jeffrey, N., Cranmer, M., Ho, S. & Battaglia, P. Rediscovering orbital mechanics with machine learning. *Machine Learning: Science And Technology*. **4**, 045002 (2023)
- [45] Liu, Z. & Tegmark, M. Machine learning conservation laws from trajectories. *Physical Review Letters*. **126**, 180604 (2021)
- [46] Liu, Z., Madhavan, V. & Tegmark, M. Machine learning conservation laws from differential equations. *Physical Review E*. **106**, 045307 (2022)
- [47] Alet, F., Doblár, D., Zhou, A., Tenenbaum, J., Kawaguchi, K. & Finn, C. Noether networks: meta-learning useful conserved quantities. *Advances In Neural Information Processing Systems*. **34** pp. 16384-16397 (2021)
- [48] Udrescu, S. & Tegmark, M. AI Feynman: A physics-inspired method for symbolic regression. *Science Advances*. **6**, eaay2631 (2020)
- [49] Udrescu, S., Tan, A., Feng, J., Neto, O., Wu, T. & Tegmark, M. AI Feynman 2.0: Pareto-optimal symbolic regression exploiting graph modularity. *Advances In Neural Information Processing Systems*. **33** pp. 4860-4871 (2020)
- [50] Fronk, C. & Petzold, L. Interpretable polynomial neural ordinary differential equations. *Chaos: An Interdisciplinary Journal Of Nonlinear Science*. **33** (2023)
- [51] Cornelio, C., Dash, S., Austel, V., Josephson, T., Goncalves, J., Clarkson, K., Megiddo, N., El Khadir, B. & Horesh, L. Combining data and theory for derivable scientific discovery with AI-Descartes. *Nature Communications*. **14**, 1777 (2023)
- [52] Karniadakis, G., Kevrekidis, I., Lu, L., Perdikaris, P., Wang, S. & Yang, L. Physics-informed machine learning. *Nature Reviews Physics*. **3**, 422-440 (2021)
- [53] Sharma, P., Chung, W., Akoush, B. & Ihme, M. A review of physics-informed machine learning in fluid mechanics. *Energies*. **16**, 2343 (2023)
- [54] Cuomo, S., Di Cola, V., Giampaolo, F., Rozza, G., Raissi, M. & Piccialli, F. Scientific machine learning through physics-informed neural networks: Where we are and what's next. *Journal Of Scientific Computing*. **92**, 88 (2022)
- [55] Brunton, S., Noack, B. & Koumoutsakos, P. Machine learning for fluid mechanics. *Annual Review Of Fluid Mechanics*. **52**, 477-508 (2020)

- [56] Hernández, Q., Badiás, A., Chinesta, F. & Cueto, E. Port-metriplectic neural networks: thermodynamics-informed machine learning of complex physical systems. *Computational Mechanics*. **72**, 553-561 (2023)
- [57] Breen, P., Foley, C., Boekholt, T. & Zwart, S. Newton versus the machine: solving the chaotic three-body problem using deep neural networks. *Monthly Notices Of The Royal Astronomical Society*. **494**, 2465-2470 (2020)
- [58] Xiong, W., Ma, M., Huang, X., Zhang, Z., Sun, P. & Tian, Y. Koopmanlab: machine learning for solving complex physics equations. *APL Machine Learning*. **1** (2023)
- [59] Sanchez-Gonzalez, A., Godwin, J., Pfaff, T., Ying, R., Leskovec, J. & Battaglia, P. Learning to simulate complex physics with graph networks. *International Conference On Machine Learning*. pp. 8459-8468 (2020)
- [60] Zobeiry, N. & Humfeld, K. A physics-informed machine learning approach for solving heat transfer equation in advanced manufacturing and engineering applications. *Engineering Applications Of Artificial Intelligence*. **101** pp. 104232 (2021)
- [61] Willard, J., Jia, X., Xu, S., Steinbach, M. & Kumar, V. Integrating scientific knowledge with machine learning for engineering and environmental systems. *ACM Computing Surveys*. **55**, 1-37 (2022)
- [62] Bismukhametov, T. & Jäschke, J. Combining machine learning and process engineering physics towards enhanced accuracy and explainability of data-driven models. *Computers & Chemical Engineering*. **138** pp. 106834 (2020)
- [63] Greydanus, S., Dzamba, M. & Yosinski, J. Hamiltonian neural networks. *Advances In Neural Information Processing Systems*. **32** (2019)
- [64] Cranmer, M., Greydanus, S., Hoyer, S., Battaglia, P., Spergel, D. & Ho, S. Lagrangian neural networks. *ArXiv Preprint [arXiv:2003.04630](https://arxiv.org/abs/2003.04630)*. (2020)
- [65] Liu, Z., Wang, B., Meng, Q., Chen, W., Tegmark, M. & Liu, T. Machine-learning nonconservative dynamics for new-physics detection. *Physical Review E*. **104**, 055302 (2021)
- [66] Sosanya, A. & Greydanus, S. Dissipative hamiltonian neural networks: Learning dissipative and conservative dynamics separately. *ArXiv Preprint [arXiv:2201.10085](https://arxiv.org/abs/2201.10085)*. (2022)

- [67] Lim, Y. & Kasim, M. Unifying physical systems' inductive biases in neural ODE using dynamics constraints. *ArXiv Preprint arXiv:2208.02632*. (2022)
- [68] Defining physicists' relationship with AI. *Nature Reviews Physics* **4**, 735 (2022). <https://doi.org/10.1038/s42254-022-00544-1>
- [69] Einstein, A. Science and religion. (Conference on Science, Philosophy,1940)
- [70] Raissi, M., Perdikaris, P. & Karniadakis, G. Multistep neural networks for data-driven discovery of nonlinear dynamical systems. *ArXiv Preprint arXiv:1801.01236*. (2018)
- [71] Long, Z., Lu, Y. & Dong, B. PDE-Net 2.0: Learning PDEs from data with a numeric-symbolic hybrid deep network. *Journal Of Computational Physics*. **399** pp. 108925 (2019)
- [72] Rudy, S., Brunton, S., Proctor, J. & Kutz, J. Data-driven discovery of partial differential equations. *Science Advances*. **3**, e1602614 (2017)
- [73] Schrödinger, E. An undulatory theory of the mechanics of atoms and molecules. *Physical Review*. **28**, 1049 (1926)
- [74] Chen, R., Rubanova, Y., Bettencourt, J. & Duvenaud, D. Neural ordinary differential equations. *Advances In Neural Information Processing Systems*. **31** (2018)
- [75] Takeishi, N. & Kalousis, A. Physics-integrated variational autoencoders for robust and interpretable generative modeling. *Advances In Neural Information Processing Systems*. **34** pp. 14809-14821 (2021)
- [76] Choi, M., Flam-Shepherd, D., Kyaw, T. & Aspuru-Guzik, A. Learning quantum dynamics with latent neural ordinary differential equations. *Physical Review A*. **105**, 042403 (2022)
- [77] Lai, Z., Liu, W., Jian, X., Bacsá, K., Sun, L. & Chatzi, E. Neural modal ordinary differential equations: Integrating physics-based modeling with neural ordinary differential equations for modeling high-dimensional monitored structures. *Data-Centric Engineering*. **3** pp. e34 (2022)
- [78] Sholokhov, A., Liu, Y., Mansour, H. & Nabi, S. Physics-informed neural ODE (PIN-ODE): embedding physics into models using collocation points. *Scientific Reports*. **13**, 10166 (2023)

- [79] Daniels, B. & Nemenman, I. Automated adaptive inference of phenomenological dynamical models. *Nature Communications*. **6**, 8133 (2015)
- [80] Kingma, D. & Welling, M. Auto-encoding variational bayes. *ArXiv Preprint arXiv:1312.6114*. (2013)
- [81] Zhao, S., Song, J. & Ermon, S. Infovae: Information maximizing variational autoencoders. *ArXiv Preprint arXiv:1706.02262*. (2017)
- [82] Yang, Z., Zhang, S., Hu, Y., Hu, Z. & Huang, Y. VAE-Stega: linguistic steganography based on variational auto-encoder. *IEEE Transactions On Information Forensics And Security*. **16** pp. 880-895 (2020)
- [83] Jiao, P., Guo, X., Jing, X., He, D., Wu, H., Pan, S., Gong, M. & Wang, W. Temporal network embedding for link prediction via VAE joint attention mechanism. *IEEE Transactions On Neural Networks And Learning Systems*. **33**, 7400-7413 (2021)
- [84] Higgins, I., Matthey, L., Pal, A., Burgess, C., Glorot, X., Botvinick, M., Mohamed, S. & Lerchner, A. beta-vae: Learning basic visual concepts with a constrained variational framework.. *ICLR (Poster)*. **3** (2017)
- [85] Asperti, A. & Trentin, M. Balancing reconstruction error and kullback-leibler divergence in variational autoencoders. *Ieee Access*. **8** pp. 199440-199448 (2020)
- [86] Xu, J. & Durrett, G. Spherical latent spaces for stable variational autoencoders. *ArXiv Preprint arXiv:1808.10805*. (2018)
- [87] Nicolau, M., McDermott, J. & Others Learning neural representations for network anomaly detection. *IEEE Transactions On Cybernetics*. **49**, 3074-3087 (2018)
- [88] Cho, K., Van Merriënboer, B., Gulcehre, C., Bahdanau, D., Bougares, F., Schwenk, H. & Bengio, Y. Learning phrase representations using RNN encoder-decoder for statistical machine translation. *ArXiv Preprint arXiv:1406.1078*. (2014)
- [89] Zhou, J., Cui, G., Hu, S., Zhang, Z., Yang, C., Liu, Z., Wang, L., Li, C. & Sun, M. Graph neural networks: A review of methods and applications. *AI Open*. **1** pp. 57-81 (2020)
- [90] Brunton, S., Budišić, M., Kaiser, E. & Kutz, J. Modern Koopman theory for dynamical systems. *ArXiv Preprint arXiv:2102.12086*. (2021)

- [91] Gu, Z., Yan, Y. & Wu, S. Neural ODEs for holographic transport models without translation symmetry. *ArXiv Preprint [arXiv:2401.09946](https://arxiv.org/abs/2401.09946)*. (2024)
- [92] Rrapaj, E., Patwardhan, A., Armstrong, E. & Fuller, G. Inference of neutrino flavor evolution through data assimilation and neural differential equations. *Physical Review D*. **103**, 043006 (2021)
- [93] Li, Q., Wang, T., Roychowdhury, V. & Jawed, M. Metalearning generalizable dynamics from trajectories. *Physical Review Letters*. **131**, 067301 (2023)
- [94] Yin, Y., Le Guen, V., Dona, J., Bézenac, E., Ayed, I., Thome, N. & Gallinari, P. Augmenting physical models with deep networks for complex dynamics forecasting. *Journal Of Statistical Mechanics: Theory And Experiment*. **2021**, 124012 (2021)
- [95] Guen, V. & Thome, N. Disentangling physical dynamics from unknown factors for unsupervised video prediction. *Proceedings Of The IEEE/CVF Conference On Computer Vision And Pattern Recognition*. pp. 11474-11484 (2020)
- [96] Zhou, D. & Wei, X. Learning identifiable and interpretable latent models of high-dimensional neural activity using pi-VAE. *Advances In Neural Information Processing Systems*. **33** pp. 7234-7247 (2020)
- [97] Frohnert, F. & Nieuwenburg, E. Explainable representation learning of small quantum states. *Machine Learning: Science And Technology*. **5**, 015001 (2024)
- [98] Monteiro, M., Le Folgoc, L., Castro, D., Pawlowski, N., Marques, B., Kamnitsas, K., Wilk, M. & Glocker, B. Stochastic segmentation networks: Modelling spatially correlated aleatoric uncertainty. *Advances In Neural Information Processing Systems*. **33** pp. 12756-12767 (2020)
- [99] Rumelhart, D., Hinton, G. & Williams, R. Learning representations by back-propagating errors. *Nature*. **323**, 533-536 (1986)
- [100] Hsu, W., Dutta, D. & Helmy, A. Structural Analysis of User Association Patterns in Wireless LAN. *ArXiv Preprint [cs/0606002](https://arxiv.org/abs/cs/0606002)*.
- [101] Finlay, C., Jacobsen, J., Nurbekyan, L. & Oberman, A. How to train your neural ODE: the world of Jacobian and kinetic regularization. *International Conference On Machine Learning*. pp. 3154-3164 (2020)

- [102] Iakovlev, V., Yildiz, C., Heinonen, M. & Lähdesmäki, H. Latent Neural ODEs with Sparse Bayesian Multiple Shooting. *The Eleventh International Conference On Learning Representations*.
- [103] Morrill, J., Kidger, P., Salvi, C., Foster, J. & Lyons, T. Neural cdes for long time series via the log-ode method. (2020)
- [104] Anderson, P. Absence of diffusion in certain random lattices. *Physical Review*. **109**, 1492 (1958)
- [105] Cutler, M. & Mott, N. Observation of Anderson localization in an electron gas. *Physical Review*. **181**, 1336 (1969)
- [106] Papadopoulos, G. Exact evaluation of a path integral relating to an electron gas in a random potential. *Journal Of Physics A: Mathematical, Nuclear And General*. **7**, 183 (1974)
- [107] Lye, J., Fallani, L., Modugno, M., Wiersma, D., Fort, C. & Inguscio, M. Bose-Einstein condensate in a random potential. *Physical Review Letters*. **95**, 070401 (2005)
- [108] Cherroret, N. & Skipetrov, S. Long-Range Correlations of Density in a Bose-Einstein Condensate Expanding in a Random Potential. *Physical Review Letters*. **101**, 190406 (2008)
- [109] Tsitouras, C. Runge–Kutta pairs of order 5 (4) satisfying only the first column simplifying assumption. *Computers & Mathematics With Applications*. **62**, 770-775 (2011)
- [110] He, K., Zhang, X., Ren, S. & Sun, J. Delving deep into rectifiers: Surpassing human-level performance on imagenet classification. *Proceedings Of The IEEE International Conference On Computer Vision*. pp. 1026-1034 (2015)